Publ. Astron. Soc. Japan **41**, 937–952 (1989)

CO Observations of the Interacting Edge-on Galaxy NGC 4631: Fission or Double Ring?*

Yoshiaki SOFUE and Toshihiro HANDA

Institute of Astronomy, The University of Tokyo, Mitaka, Tokyo 181

and

Naomasa NAKAI

Nobeyama Radio Observatory, Minamimaki-mura, Minamisaku-gun, Nagano 384-13

(Received 1989 April 15; accepted 1989 June 2)

Abstract

The interacting edge-on galaxy NGC 4631 was observed in the ^{12}CO ($J=1-0$) line using the Nobeyama 45-m telescope. The molecular gas is strongly concentrated in the inner region of 1-kpc radius and shows a rigid rotation. Four intensity peaks of the CO emission have been identified along the major axis, located symmetrically with respect to the center and positionally coinciding with radio continuum peaks. Two possible models are considered to explain the CO peaks. (i) In the double-ring model, they are interpreted in terms of two rings of molecular hydrogen gas of radii 250 pc and 1 kpc. The rings are rotating at velocities of 20 and 80 km s^{-1}, respectively, much slower than the galactic rotation (150 km s^{-1}) of the outer disk, and no expanding motion has been detected. The rings are warped with respect to the optically determined major axis. The formation mechanism of the double gaseous rings in a bar potential caused by a tidal interaction with the companion galaxy NGC 4656 is discussed. (ii) In the fission model, the CO peaks are interpreted as being clumps of molecular gas formed as the result of a fission of the central gas disk which forms by a bar-induced gas inflow, where the bar is formed by a tidal encounter with the companion NGC 4656. The deviation of radial velocities from rigid rotation is consistent with the fission model.

Key words: CO emission; Edge-on galaxies; Fission; Gaseous rings; Molecular hydrogen; Tidal interaction.

* Based on observations made at the Nobeyama Radio Observatory (NRO). NRO is a branch of the National Astronomical Observatory, an inter-university research institute operated by the Ministry of Education, Science, and Culture.

1. Introduction

NGC 4631 (Arp 281) is a late-type galaxy seen nearly edge-on. It was classified as being an Sc-type galaxy by E. Hubble (Sandage 1961); it has also been classified as being a Magellanic-type barred spiral galaxy (de Vaucouleurs and de Vaucouleurs 1963) or an SBd galaxy (de Vaucouleurs et al. 1976). The galaxy appears to be distorted, which may be due to an interaction with a nearby small elliptical galaxy, NGC 4627, at an angular separation of 2.5 and/or with its companion galaxy, NGC 4656, at an angular separation of 40′. This led Arp (1966) to include the galaxy in his *Atlas of Peculiar Galaxies* as No. 281. Sandage and Tammann (1974) give the distance to this galaxy as being 5.2 Mpc, corresponding to a scale of 1 kpc/40″. An optical photograph (e.g., de Bruyn 1977) shows a patchy dust lane along the major axis, suggesting the existence of a wealth of molecular gas. However, no clear nucleus can be recognized, giving an uncertain position of the galactic center. The galaxy is bright in the far-infrared emission, as observed by IRAS, while no evidence for starbursts has been reported.

Radio continuum observations (Klein et al. 1984) have indicated a bright disk component near the center, almost two orders of magnitude brighter than the outer disk component. High-resolution observations at 6 cm with the WSRT (de Bruyn 1977) have shown that this nuclear radio disk contains a complex elongated structure with a linear dimension of about 2.5 kpc (100″): the disk is composed of a central component and two peaks symmetrically located 1 kpc from the center. The central component is resolved into two peaks which are situated symmetrically with respect to the nucleus at a distance of about 250 pc from the center. At lower frequencies the galaxy has an extended diffuse emission of a few kpc thickness, which suggests the existence of a dynamic halo with high-energy particles supplied from the disk and/or from the nuclear region (Ekers and Sancisi 1977; Werner 1985; Hummel et al. 1988). Continuum observations at 327 MHz (Sukumar and Velusamy 1985) indicate double-lobe features at about 7 kpc above and below the center, suggesting some ejection from the nuclear region.

H I observations (Weliachew et al. 1978) have revealed the presence of several filamentary features extending for tens of kiloparsecs from the galactic center, one of which composes a bridge connecting NGC 4631 and NGC 4656. This H I bridge and the distorted optical morphology of NGC 4631 suggest a strong tidal interaction which has been well reproduced by a numerical simulation (Combes 1978). It is shown that such a gravitational disturbance causes a dynamical effect within the disk of the perturbed galaxy and produces a self-sustaining bar; the bar leads to an accretion of gas toward the center, making a dense nuclear gas disk (Noguchi 1987, 1988). The bright radio disk in the inner 1 kpc region of NGC 4631 could be accounted for by the existence of such a nuclear dense gas disk.

Direct evidence for such a nuclear gas disk may be obtained by observing the ^{12}CO ($J=1-0$) line emission of the galaxy. In this paper we report the result of observations of the ^{12}CO ($J=1-0$) line emission toward NGC 4631 using the Nobeyama 45-m telescope. We discuss the observed CO emission features based on two possible models: a double-ring model and a fission model.

Table 1. Adopted parameters for NGC 4631.

Type[1,2]	Sc/SBd
Inclination	Edge-on
Position angle of major axis	86°.5
Distance[3]	5.2 Mpc
Center position[4] ($X=0''$, $Y=0''$)	$\alpha_{1950}=12^h30^m41^s.0$
	$\delta_{1950}=32°48'58''$
Systemic LSR velocity[4]	617 km s^{-1}

(1) Sandage (1961); (2) de Vaucouleurs et al. (1976); (3) Sandage and Tammann (1974); (4) Weliachew et al. (1978): the center position is about 2″ south of that given in the literature.

2. Observations

Observations of the ^{12}CO ($J=1-0$) line of NGC 4631 were made on Feb. 22 through 25, 1989, using the 45-m telescope of the Nobeyama Radio Observatory. The antenna had a HPBW of 17″, corresponding to a linear scale of 425 pc. The pointing accuracy was better than $\pm 3''$ through the observations. The main-beam and forward spillover-and-scattering efficiencies were $\eta_{mb}=43\%$ and $\eta_{fss}\equiv\eta_{Moon}=75\%$, respectively. We used a cooled Schottky-barrier diode mixer receiver combined with a 2048-channel acousto-optical spectrometer of 250-MHz bandwidth, which covered 650 km s^{-1} with a velocity resolution of 0.6 km s^{-1} and channel separation of 0.32 km s^{-1}. We binded every 32 channels, which yielded a final velocity resolution of 10.2 km s^{-1}, in order to increase the signal-to-noise ratio. The system noise temperature at the observing elevations was about 1000 K. The used intensity scale was the antenna temperature, T_A^*, corrected for the atmospheric loss.

We used a position-switching mode with multiple (six) on-positions and two off-positions at offsets of $\pm 5'$ from the galaxy center in declination (in the direction almost perpendicular to the major axis of the galaxy). We observed all points in two separate series of runs and added them after the observation. The total integration time per data point was about 6 min. The rms noise of the resultant spectra of 10 km s^{-1} velocity resolution was about $\Delta T_A^* \simeq 20$ mK.

In order to determine the reference center position, we observed the central region for a few hours at the beginning of observations, and chose a point where the ^{12}CO ($J=1-0$) intensity attains a maximum across the galactic plane and the velocity profile becomes symmetric with respect to the adopted systemic LSR velocity. We chose the center position to be $\alpha_{1950}=12^h30^m41^s.0$, $\delta_{1950}=32°48'58''$, which coincides with the center position adopted by Weliachew et al. (1978) within 2″. The systemic LSR velocity was adopted from the H I observations by Weliachew et al. (1978), who gave a heliocentric velocity of 610 ± 10 km s^{-1}, corresponding to $V_{LSR}=617$ km s^{-1}. Adopted parameters are summarized in table 1.

The major axis of the galaxy is taken at PA = 86°.5 from an optical photograph (e.g., de Bruyn 1977); the major axis is approximately in the direction of E and W. In the following we take a coordinate system (X, Y) with its origin at the center position given above. The coordinate X is taken along the major axis and Y perpendicular to it ($X>0$ toward E and $Y>0$ toward N). We observed the major axis for

$-100'' < X < +100''$ (within ± 2.5 kpc from center) at a grid spacing of $10''$ and three strips parallel to the major axis at $Y = +10''$, $-10''$, and $-20''$ for $-50'' < X < +50''$ with the same spacing.

3. Results

(a) Spectra

Figure 1 shows the obtained ^{12}CO ($J=1-0$) line spectra along the major axis. The CO line is well detected in the inner $\pm 50''$ (within 1.3 kpc). The line profile at the center is symmetric with respect to the systemic velocity and has a high-velocity tail reaching ± 100 km s^{-1}. However, the line width, about 100 km s^{-1} at the half maxima, is narrow for a galactic center when compared with those observed in our Galaxy and in the edge-on galaxy NGC 891 (Sofue et al. 1987). The intensity increases with the distance from the center up to $X = \pm 50''$, while the velocity width becomes narrower. The highest temperatures of $T_A^* \simeq 0.2$ K were observed toward $X \simeq \pm 30-40''$ (750–1000 pc). Clear red shifts of the profiles were observed at $X > 0''$, and blue shifts at $X < 0''$, indicating rotation about the adopted center. Beyond a distance of $50''$ the line intensity decreased suddenly, and no significant emission was detected at $|X| > 70''$.

Line profiles at $Y = \pm 10''$ are similar to those obtained at $Y = 0''$, while the intensities are less. The intensity distribution as a function of X is not symmetric for both strips at $Y = \pm 10''$. A comparison of the profiles off the major axis and that along the major axis is made using position-velocity diagrams in subsection (c). The emission at $|Y| > 20''$ is much weaker than that along the other three strips, indicating a thin CO disk.

(b) Intensity Distribution and H_2 Mass

The integrated intensity, $I \equiv \int T_A^* dv$, is plotted in figure 2 as a function of X. The distribution has three major peaks, one near the center and the other two at $X \simeq \pm 30$–$40''$, symmetrically opposite to each other with respect to the center.

The column density of the molecular hydrogen (H_2) gas averaged within the beam area (HPBW = 425 pc) can be estimated from the CO intensity as

$$N_{H_2}\,[\mathrm{H_2\,cm^{-2}}] \sim 4 \times 10^{20} \int T_R^* dv \sim 6 \times 10^{20} I\,[\mathrm{K\,km\,s^{-1}}]\,.$$

Here, $T_R^* \equiv T_A^*/\eta_{fss}$ with $\eta_{fss} \simeq 0.75$, which applies for the case when the object is more extended than the telescope beam. The conversion factor from the CO intensity to H_2 mass was taken from the empirical relation obtained for galactic molecular clouds (Young and Scoville 1982) by correcting for the difference of efficiencies between the NRAO 11-m telescope and the 45-m telescope. The conversion factor, and therefore the H_2 mass, are uncertain by a factor of two. [Note that T_A^* used in Young and Scoville (1982) was actually T_R^* (Kutner and Ulich 1981; Young et al. 1986).] The surface mass density of the molecular gas averaged within the beam is then given by

$$\sigma\,[M_\odot\,\mathrm{pc^{-2}}] \sim 10 \times I\,[\mathrm{K\,km\,s^{-1}}]\,.$$

The variation of the CO intensity across the major axis (galactic plane) indicates that the CO gas layer is thin enough compared to the beam width, $17''$ (425 pc). This

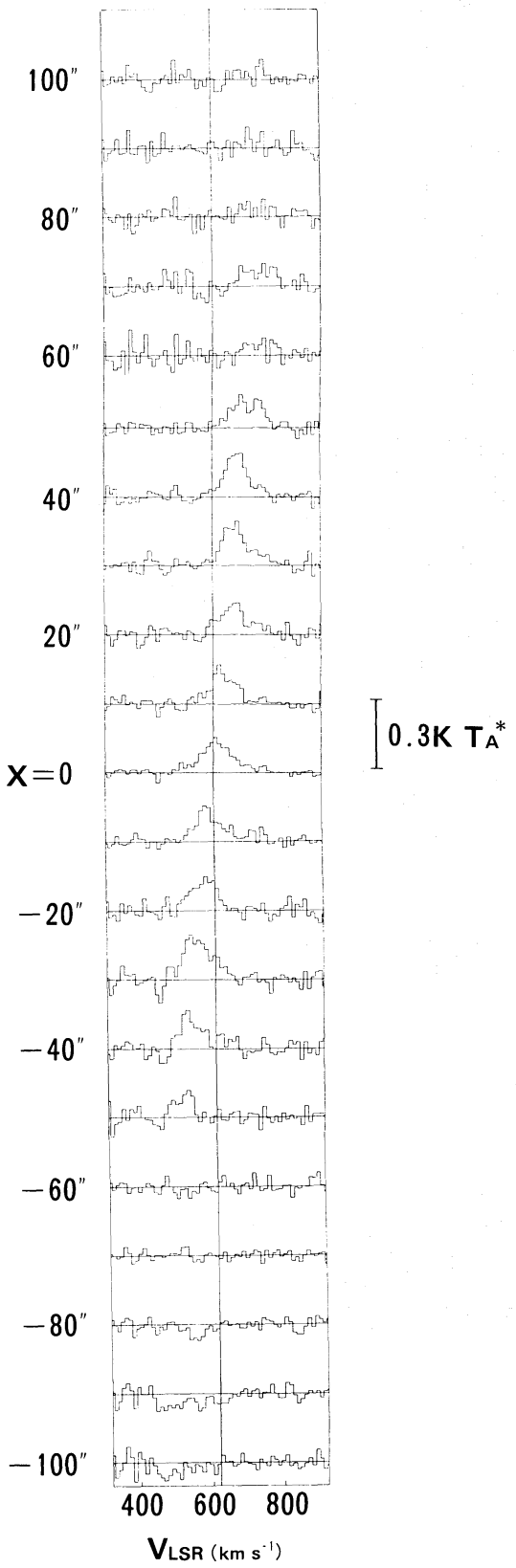

Fig. 1. Spectra of the ^{12}CO ($J=1-0$) line of the edge-on galaxy NGC 4631 along the major axis with X being the distance from the center toward the east, as observed with the 45-m telescope.

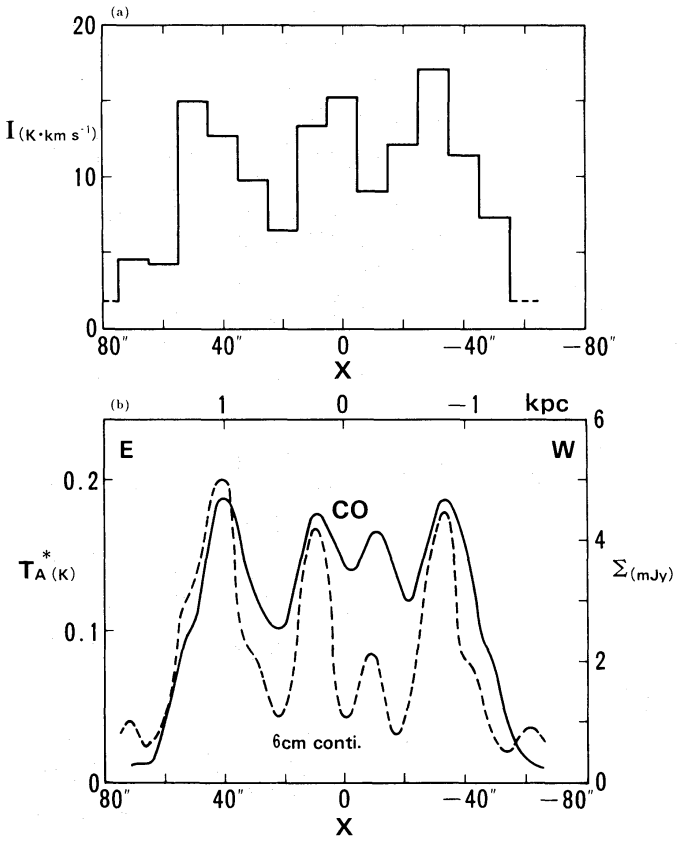

Fig. 2. (a) The distribution of the CO intensity along the major axis of NGC 4631. (b) The distribution along the major axis of the peak antenna temperature (thick line) as read from the X-V_{LSR} diagram in figure 4, and the distribution of the brightness temperature of the radio continuum emission at 6 cm along the major axis [dashed line: de Bruyn (1977)].

is consistent with the edge-on nature of a spiral galaxy whose molecular gas layer usually has a scale thickness of about 100 pc or less. This fact allowed us to estimate the approximate total H_2 mass from the one-dimensional scan along the major axis: The total mass of H_2 gas in the observed region of $|X|<100''$ (2.5 kpc) was obtained to be $M_{H_2}\sim 1.4\times 10^8 M_\odot$. More than 90% of the mass or about $1.3\times 10^8 M_\odot$ is confined within the disk of radius 1.3 kpc ($|X|<50''$). If the molecular gas is distributed in a disk of thickness $\sim$100 pc, the mean density of gas within the disk of radius 1 kpc is approximately given by

$$\langle \rho_{gas}\rangle \sim 18\,\mathrm{H\,cm^{-3}}\,.$$

No significant emission was found at $2.5>|X|>\sim 1.3$ kpc, where $T_A^*<3\Delta T_A^*\simeq 0.06$ K. This put an upper limit on the CO intensity as $I<3\times\Delta T_A^*[\Delta V\cdot w]^{1/2}\sim 2$ K km s^{-1}, where $\Delta V=10$ km s^{-1} and $w\sim 100$ km s^{-1} are the velocity resolution and an expected line width, respectively. This intensity limit gives an upper limit to the mass involved in the strips along the line of sights at $2.5>X>1.3$ and $-2.5<X<-1.3$ kpc to be $M_{H_2}<1.5\times 10^7 M_\odot$. Since the galaxy is edge-on and we are looking through the disk from the foreground edge to behind, this limit allows us a rough estimation of an upper limit to the H_2 mass beyond $|X|=2.5$ kpc and within a certain radius, say within

the Holmberg radius (~ 14 kpc): this is approximately given by $M_{H_2}[2.5 < R < 14\,\mathrm{kpc}] < \sim 1.5 \times 10^8 M_\odot$. Namely, the total H_2 mass in NGC 4631 is estimated to be less than $\sim 3 \times 10^8 M_\odot$. The H_2 mass should be compared with the H I mass, $M_{HI} \sim 3.2 \times 10^9 M_\odot$, and the total dynamical mass, $M_T \sim 5.7 \times 10^{10} M_\odot$, within 14 kpc radius (Weliachew et al. 1978).

(c) Position-Velocity Diagrams and the Galactic Rotation

A position-velocity diagram along the major axis is shown in figure 3, where the distribution of the antenna temperature, T_A^*, is indicated on the X-V_{LSR} plane in the form of contour diagram. Figure 4 is the same, but the diagram for the inner 50″ is enlarged. Figures 5a to 5c compare the X-V_{LSR} diagrams along the three strips at $Y = +10''$, $0''$, and $-10''$.

The obtained position-velocity diagrams indicate a clear rotation of the central molecular disk. For an edge-on galaxy the rotation characteristics may be derived without any uncertainty in the inclination. The CO observations will better represent the rotation characteristics in the inner few kpc than the H I observations (Weliachew et al. 1978), not only for better resolution but also due to the fact that the molecular gas is more concentrated in the inner region than H I gas.

Beyond the nucleus the rotation velocity V increases almost linearly with the radius R,

$$V(R)\,[\mathrm{km\,s^{-1}}] \simeq 80 R\,[\mathrm{kpc}]\,.$$

The H I observations (Weliachew et al. 1978) show that the velocity increases up to $V \simeq 150\,\mathrm{km\,s^{-1}}$ at $R \sim 2$ kpc, reaching a flat rotation thereafter. Such a rigid rotation at $R < 1$–2 kpc is often observed for Sc galaxies (Rubin et al. 1980): the common Sc rotation velocity rises rapidly within a few kpc, and more slowly thereafter, reaching a flat (differential) rotation.

The X-V_{LSR} diagram along the galactic plane ($Y = 0$) is symmetric with respect to the center. However, those along strips off the plane ($Y = \pm 10''$) show significant asymmetry (figure 5). Above the galactic plane, or at positive Y, the gas distribution appears shifted toward the east ($X > 0$), while below the plane more gas is observed in the western side ($X < 0$). Such an asymmetry could be explained if the disk of the molecular gas is warping with respect to the optical major axis. The amount of displacement in the eastern part of the disk was roughly estimated to be of the order of 100 pc toward positive Y at $X \sim 1$ kpc and vice versa in the western half. Since the optical position angle (86°.5) is accurate within $\pm 2°$, this means that the molecular disk is warped by several degrees from the optical (outer) disk toward the north in the eastern part and toward the south in the western half.

(d) Mass Distribution

If the mass is assumed to be distributed in a sphere and orbiting in circular orbits about the center, the balance of gravitational and centrifugal forces gives

$$M_{dyn}(R)\,[M_\odot] = 2.33 \times 10^5 V^2(R) R\,,$$

where $M_{dyn}(R)$ is the integral mass interior to R (in kpc), and $V(R)$ (in $\mathrm{km\,s^{-1}}$) is the

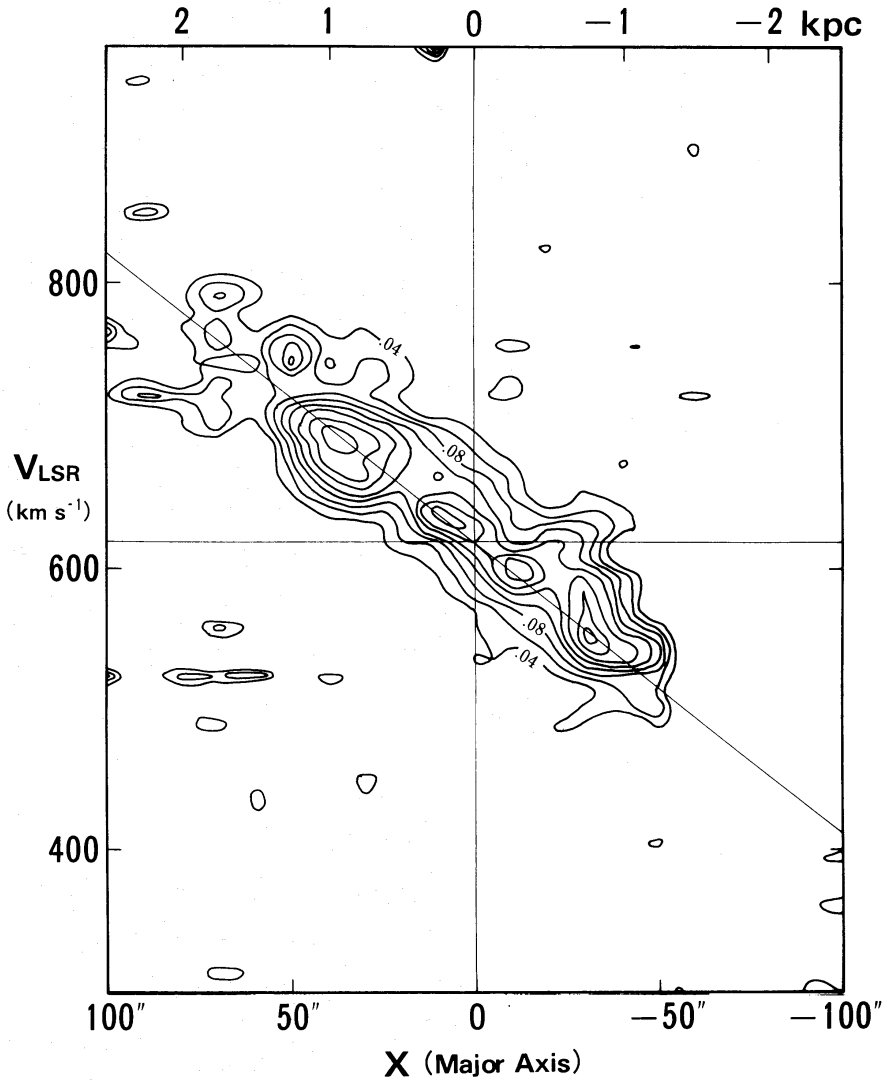

Fig. 3. Position-velocity (X-$V_{\rm LSR}$) diagram of the ^{12}CO intensity, I, obtained along the major axis of NGC 4631. Contour labels are in units of K $T_{\rm A}^{*}$: the lowest contour is at 0.04 K and the intervals are 0.02 K. Note the high concentration of gas in the inner $\sim$1 kpc and a linear rotation characteristics of the gas.

rotation velocity at R. For NGC 4631 we obtain

$$M_{\rm dyn}(R)\,[M_{\odot}] \simeq 1.49 \times 10^{9} R^{3}\ .$$

Since the mass in the central region may be dominated by the central bulge component with radius $\sim$1 kpc for an Sc galaxy, we may assume that the mass distribution is spherical at $R < 1$ kpc. Then, the mass density distribution in the region is constant and is given by

$$\rho \simeq 0.36 M_{\odot}\ {\rm pc}^{-3} = 15\ {\rm H\ atoms\ cm}^{-3}\ .$$

We note that the observed rotation characteristics indicate that there is no particular concentration of mass toward the nucleus. Such a uniform density near the center may

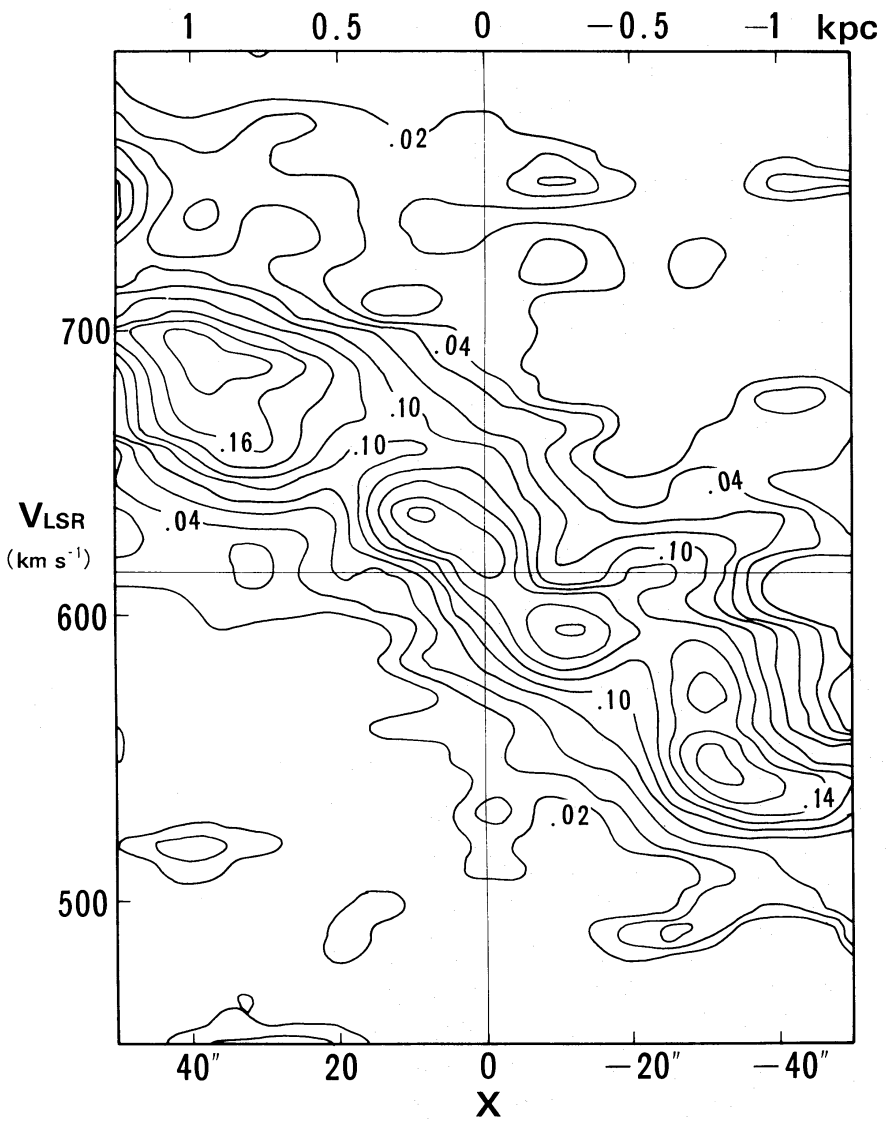

Fig. 4. Enlargement of the X-V_{LSR} diagram of I for the inner 1 kpc. The lowest contour level and the intervals are 0.02 K T_A^*. Note the two large concentrations near $(X, V_{LSR}) \simeq$ (1 kpc, 690 km s^{-1}) and (-0.8 kpc, 530 km s^{-1}) and two smaller concentrations at $(X, V_{LSR}) \simeq$ (250 pc, 640 km s^{-1}) and (-250 pc, 600 km s^{-1}).

be related to the galaxy type classified as Sc with a small central bulge and, hence, less mass near the center compared to earlier-type galaxies.

The total (dynamical) mass involved in the inner 50″ (1.3 kpc) radius, where most of the H_2 gas of mass $1.3 \times 10^8 M_\odot$ is confined, is estimated to be $2.9 \times 10^9 M_\odot$. This gives the molecular gas-to-dynamical (total) mass ratio, $\gamma = M_{H_2}/M_{dyn} \sim 0.04$ for the inner 1.3 kpc. The ratio increases toward the center: in the central 20″ region ($R <$ 500 pc), where $M_{dyn} \sim 1.9 \times 10^8 M_\odot$ and $M_{H_2} \sim 5.2 \times 10^7 M_\odot$, the ratio is as large as $\gamma \simeq 0.27$. Moreover, the density ratio of the gas-to-dynamical mass in the disk should be larger than the above ratios: In a molecular gas disk, where the gas is confined within a layer of $\sim$100 pc thickness, the ratio of the densities is estimated to be $\gamma_{disk} =$

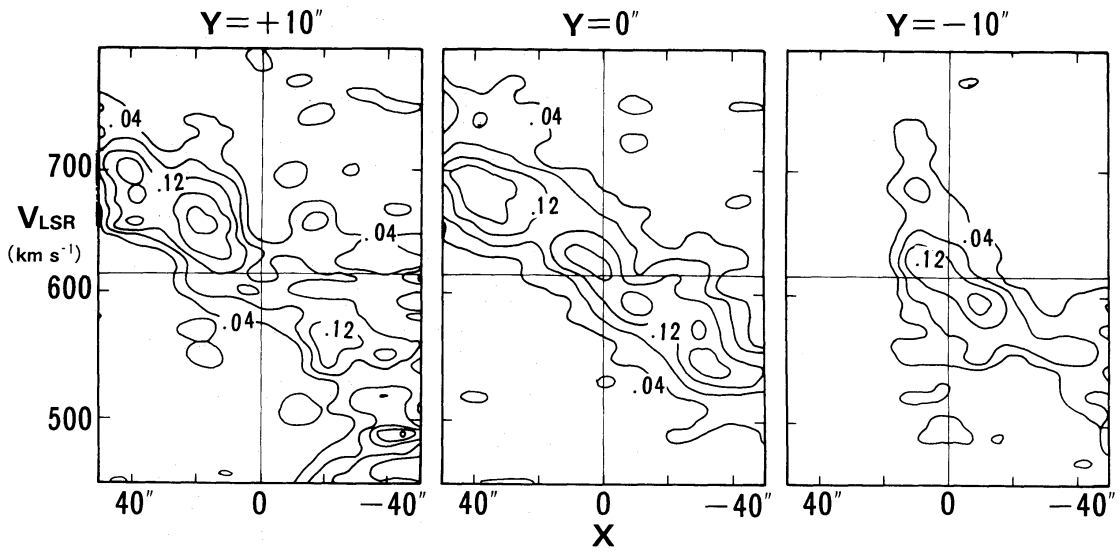

Fig. 5. Comparison of the X-V_{LSR} diagrams at $Y=+10''$, $0''$, and $-10''$. Note the asymmetry of the distributions above and below the galactic plane, which may be due to warping of the nuclear disk. The lowest contour level and the intervals are 0.04 K T_A^*.

$\rho_{gas}/\rho_{dyn} \sim 1$ at $R<1$ kpc; the value is larger in more inner regions.

(e) Rotating Rings or Fission?

The intensity distribution given in figure 2 shows that the molecular gas disk is composed of three remarkable peaks: (i) two peaks at $X \simeq \pm 1$ kpc, which appear symmetrically with respect to the center, and which we call the "1-kpc feature", and (ii) a central peak with the emission concentrated within a few hundred pc. The double-peak component can be interpreted either as being a molecular gas ring of radius 1 kpc and width 200 pc rotating at 80 km s^{-1}, or by a double-clump structure which is expected if fission took place in the nuclear gas disk. This structure can be seen better in position-velocity diagrams (figures 3 and 4), which show two concentrations of gas at $(X, V_{LSR})=(40'', 690\ \text{km s}^{-1})$ and $(-35'', 530\ \text{km s}^{-1})$.

The central component cannot be a local fluctuation of the 1-kpc feature, since its high intensity is comparable to that of the double peaks. A detailed inspection into the position-velocity diagrams (figures 3 and 4) reveals that this component can be further resolved into two peaks at $(X, V_{LSR})=(10'', 640\ \text{km s}^{-1})$ and $(-10'', 600\ \text{km s}^{-1})$. Because their appearance is again symmetric about the center, the two peaks may be reasonably interpreted either by an inner ring of radius 250 pc rotating at a velocity of 20 km s^{-1} or by double clumps. We call the inner peaks the "250-pc feature". In order to see the double ring/clump structures more clearly figure 2b shows plots of the peak antenna temperatures as read from the X-V_{LSR} diagram as a function of the distance from the center. In this figure we can recognize four peaks corresponding to these features.

4. Discussion

(a) Accretion of Gas by a Tidal Interaction with NGC 4656

The present ^{12}CO ($J=1-0$) observations covered the central 5-kpc strip along the

galactic plane (within $\pm 100'' = \pm 2.5$ kpc) of the edge-on galaxy NGC 4631. The observations show that the molecular gas of mass $1.3 \times 10^8 M_\odot$ is confined within the nuclear disk of radius 1.3 kpc. The H_2 gas concentration in the nuclear region, showing a high contrast to the surrounding disk, seems to be different from the previously known CO disks of Sc galaxies like NGC 6946 and IC 342 (Young and Scoville 1982; Sofue et al. 1988; Weliachew et al. 1988): in these galaxies the central CO disks have a strong nuclear concentration whose density monotonically increases toward the center without any significant discontinuity from the outer exponential-law disk.

The high concentration of molecular gas near the center might be related to a tidal disturbance through an encounter with companion galaxy NGC 4656, which is indicated from the distorted morphology and H I bridges between the two galaxies (Weliachew et al. 1978; Combes 1978). A numerical simulation of two self-gravitating stellar systems (Noguchi 1988) has shown that the tidal encounter triggers a rapid formation of a bar which becomes a self-sustaining structure for tens of rotations in the perturbed galaxy. Note that de Vaucouleurs et al. (1976) classified NGC 4631 as a late-type barred spiral.

Once a bar forms, the non-axisymmetric potential causes galactic shocks in the interstellar gas (Sørensen et al. 1976; Huntley et al. 1978) and/or results in a transfer of angular momentum (Noguchi 1988). This will result in a rapid accretion of molecular gas toward the inner region. In fact, the typical barred spiral galaxy M83 has a high concentration of H_2 gas near the center, while only a small amount of gas is present along the major part of the bar (Handa et al. 1990).

(b) Ring Model

If we interpret the double-peak structures in the intensity distribution of the CO emission as a manifestation of the existence of molecular rings, several mechanisms may be considered for their formation:

Clouds friction: Friction due to collisions among giant molecular clouds via the differential galactic rotation, even if they are in circular orbits, causes a radial transfer of angular momentum and brings the gas toward a radius where the rotation curve turns quickly (Fukunaga 1983). In the case of NGC 4631 the turning point of the rotation curve is beyond the radius of the outer ring. Moreover, rotation near the rings is almost rigid, giving little friction. Hence, the friction model does not seem to apply in the present case.

Explosion and/or starburst: A snow-plow effect by shock produced by an intense energy release near the nucleus, such as due to an explosion and/or starbursts, results in the formation of a ring in the gas disk. In this case the position-velocity diagram is characterized by a large velocity dispersion and/or an elliptical feature. Such a ring structure has been found in some spiral galaxies: Our Galaxy exhibits various expanding molecular rings of radii of a few hundred pc to a few kpc (e.g., Oort 1985). Maffei 2 has been found to possess a similar expanding ring of 200 pc radius (Ishiguro et al. 1989). The starburst galaxy M82 has a 200-pc ring of molecular gas and shows a high-velocity dispersion (Nakai et al. 1987). However, the X-V_{LSR} diagram observed for NGC 4631 (figure 4) shows no such tendency. Hence, it does not seem to be convincing to attribute the molecular rings in NGC 4631 to an explosive event in the nucleus.

Bar-induced inflow: A tidal encounter by a companion galaxy induces a non-

axisymmetric potential, by which molecular clouds are gathered near the radius of the Lindblad resonance and form a ring-like concentration (Combes 1988). In this model the non-axisymmetric potential is weak and transient, so that the loss of angular momentum is small and a ring of a relatively large radius, say ~ 10 kpc, forms.

If the self-gravity in the perturbed galaxy is taken into account, the non-axisymmetric potential induced by the tidal encounter becomes a self-sustaining bar, and the potential is deeper and more elongated than expected from the gravitational force by the companion mass alone (Noguchi 1988). In this case the transfer of angular momentum is more efficient and bar-induced shock waves (e.g., Sørensen et al. 1976) will also promote an inflow of gas. The radius of the resulting ring will be about half the bar width. It is therefore likely that in such a distorted galaxy like NGC 4631 a deep barred potential is present and a ring of a smaller radius may form and become the 1-kpc ring.

Among the above three mechanisms, the bar-induced inflow mechanism seems most promising. It should be mentioned that barred spiral galaxies more often exhibit a rigid rotation than in normal spirals (Rubin et al. 1980); this agrees with the observed rigid rotation in NGC 4631. The inner ring structure (250-pc feature) might be accounted for if the high-density gas disk in the central few hundred pc, where the gas-to-dynamical mass ratio is large, becomes unstable against the bar instability to form an inner gaseous bar (Shlosman et al. 1989). This will result in the formation of another smaller ring within the inner bar by the same mechanism as for the outer ring formation.

(c) Fission Model

An alternative interpretation of the observed multi-peak structure in the CO intensity and X-$V_{\rm LSR}$ diagram, in particular the 1-kpc feature, can be made that individual peaks correspond to real clumps of molecular gas, which is expected if a fission of the gas disk is taking place in the central region of NGC 4631.

In fact, a numerical simulation (Tatematsu and Fujimoto 1989) has shown that a self-gravitating gas cloud rotating in the galactic center is easily elongated, when the cloud becomes more oblate (disk-shaped) and the density becomes slightly larger than the background mass density. Such a condition is fulfilled in the nuclear disk at $R<1$ kpc of NGC 4631 where the density ratio of gas to dynamical masses becomes close to unity, or $\gamma_{\rm disk}=\rho_{\rm gas}/\rho_{\rm dyn}\sim 1$ (section 3). Then, the non-axisymmetric cloud obtains a dynamical condition for its pear-shaped structure, which leads to an eventual fission into two objects. Fujimoto and Sørensen (1977) have shown that a rotating self-gravitating gas disk splits into two major clumps that are symmetric with respect to the center, each of which is then followed by self-gravitating contraction.

The theory predicts that the clump, which appeared after the fission, has its own internal rotation in addition to the rotation about the galactic center. As a consequence, the X-$V_{\rm LSR}$ diagram should show a higher inclination within the clump than the background rigid rotation. This will result in an elongation of the intensity distribution in the direction of the velocity axis on the X-$V_{\rm LSR}$ diagram. Such elongated features are really found in the observed X-$V_{\rm LSR}$ diagram (figure 4): The contours around the intensity peak at $(X, V_{\rm LSR})\simeq(35'', 670\,{\rm km\,s^{-1}})$ are stretched toward the lower-velocity side, and those around the peak at $(-30'', 550\,{\rm km\,s^{-1}})$ also have a similar elongation toward

larger velocity. Moreover, the elongated features appear to be roughly symmetric with respect to the center. Thus, the observed features, at least the 1-kpc features, may be explained by the fission scenario of the disk gas. In particular, the fact that the gas distribution lacks any real central concentration may be more related to this idea. The formation of the inner double peaks (the 250-pc feature) remains open for further discussion, although it might be possible that another fission can take place on a smaller scale in the central few hundred pc region.

If the observed intensity peaks at $X \sim \pm 1$ kpc are due to fission and are individual clumps, each may have a mass of $M_c \sim 5 \times 10^7 M_\odot$. Each clump has a diameter of about $2r_c \sim 300$ pc (figure 4), assuming a roughly round shape. The internal velocity dispersion and internal rotation velocity are approximately $v_\sigma \sim 30$ and $v_{rot} \sim 20\,\mathrm{km\,s^{-1}}$, respectively. We can then estimate the gravitational and internal kinetic energies as $E_{grav} = GM_c^2/r_c \sim 1.5 \times 10^{54}$ erg and $E_{kin} = (1/2)M_c[v_\sigma^2 + v_{rot}^2] \sim 7 \times 10^{53}$ erg. These estimates indicate that each clump can be in a gravitationally bound state, a reasonable assumption if the clumps are the result of fission.

It may be mentioned that the fission scenario might also explain the double-clump structure in the central molecular bars detected by high-resolution observations in IC 342 (Lo et al. 1984) and NGC 6946 (Ball et al. 1985) (Tatematsu and Fujimoto 1989): The molecular bars in these galaxies could be interpreted as being due to fission of the gas disk into two clumps by the same mechanism as discussed above. In fact the velocity field toward these clumps indicates a non-circular motion consistent with the internal rotation. If the bars in these galaxies were seen edge-on, they might appear in a similar fashion as the multi-peak gas distribution to that observed in NGC 4631.

We have discussed two possible interpretations of the observed features in the CO emission of NGC 4631: the ring model and the fission model. At the moment the observational material allows both interpretations. In order to distinguish between the models, we need more sensitive and higher-resolution maps and X-V_{LSR} diagrams.

(d) Correlation with the Radio Continuum Emission

It is interesting to compare the CO intensity distribution in figure 2b with the distribution of the radio continuum intensity at 6 cm (de Bruyn 1977), which is shown in the same figure. A remarkable coincidence is found in the positions of the continuum and CO emission peaks. It should be noted that there appears no particularly bright nucleus in the continuum emission showing a nuclear activity. It is unlikely that the continuum peak at $X \sim 10''$ is the nucleus, because this source is significantly away from the center of galactic rotation.

The following two possibilities can be considered for the CO-continuum coincidence:

(i) Since star formation rate is an increasing function of the molecular gas density, the density of newly born stars and the rate of supernova explosions are high in the molecular rings or in the clumps. Individual supernova remnants as well as the accelerated cosmic rays in the SN explosions will cause bright nonthermal radio emission from the disk in coincidence with the two rings/clumps.

(ii) The galactic-shock accretion in a barred potential followed by a rapid inflow

and compression of gas toward the center will result in a compression of magnetic fields in the galactic disk. This will amplify the magnetic field in the molecular gas rings/clumps. Cosmic rays are accelerated during compression. The cosmic rays and amplified magnetic fields will emit radio continuum emission showing the peaks in positional coincidence with the gaseous peaks.

Assuming a disk structure, we may derive the mean energy density and strength of the magnetic field on an assumption of equipartition between the magnetic field and cosmic rays responsible for the radio continuum emission, $E_{\rm mag}\sim 5\times 10^{-13}\,{\rm erg\,cm^{-3}}$ and $B\sim 3\,\mu{\rm G}$ for the inner 1-kpc region. Here, we used the continuum data at 6 cm of de Bruyn (1977) and assumed that the continuum emission comes from a layer of thickness ~ 100 pc. On the other hand the turbulent energy of the molecular gas in the same area will be of the order of $E_{\rm gas}\sim 1/2\rho_{\rm gas}v_{\rm turb}^2\sim 1.5\times 10^{-11}\,{\rm erg\,cm^{-3}}$, where we assumed a local turbulent velocity of the order of $10\,{\rm km\,s^{-1}}$. These estimates show that the magnetic energy density is much smaller than the gas energy density, $E_{\rm mag}\ll E_{\rm gas}$. This indicates that the magnetic fields and cosmic rays are passive with regard to the gas motion, confirming that the mechanism (ii) above may work. In reality, however, both mechanisms, (i) and (ii), may work simultaneously.

We mention that the dynamical state expected for the gas, cosmic rays and magnetic fields will trigger inflating instabilities (Parker 1971) of magnetic bubbles and cosmic rays from the nuclear disk. Such ejections of high-energy components toward the halo may explain the extended radio continuum features and the existence of the dynamical halo in NGC 4631. The instability could also enhance a small-scale clumping of gas in the disk and promote star formation.

(e) Star Formation and Far Infrared Emission

A measure of the star-forming activity of a galaxy is given by the far infrared luminosity. The IRAS data show that NGC 4631 has FIR fluxes of 1.82, 3.01, 51.15, and 118.60 Jy at 12, 25, 60, and 100 μm (Lonsdale et al. 1985). For the distance of 5.2 Mpc, the FIR luminosity between 12 and 100 μm is estimated to be $L_{\rm FIR}\sim 3.3\times 10^9 L_\odot$. If the FIR emission comes from the molecular disk of 1.3-kpc radius, this yields a FIR luminosity between 12 and 100 μm is estimated to be $L_{\rm FIR}\sim 3.3\times 10^9 L_\odot$. If the FIR emission comes from the molecular disk of 1.3-kpc radius, this yields a FIR luminosity-to-H_2 mass ratio, or the efficiency of star formation, to be $L_{\rm FIR}/M_{\rm H_2}\sim 25 L_\odot/M_\odot$. These values put NGC 4631 between normal galaxies and star-burst galaxies on the $L_{\rm FIR}/M_{\rm H_2}$ vs $L_{\rm FIR}$ diagram (Sanders et al. 1986): namely the galaxy has a relatively low FIR luminosity, while it has a relatively high star formation efficiency. We also note that the $L_{\rm FIR}/M_{\rm H_2}$ value (~ 25 in solar units) are higher than the mean values (12 ± 3) for isolated galaxies, while smaller than that for merging/interacting galaxies (78 ± 16) (Young 1988).

It has been suggested that a starburst is triggered by an accretion of gas due to a bar which is produced by a tidal encounter with a companion galaxy (Noguchi 1988) [see also a review by Sofue (1988)]. From the above estimates we may argue that NGC 4631 has not yet entered a full starburst phase, while the accretion of gas toward the center has proceeded to yield molecular rings or two clumps caused by fission. However, the relatively high star-formation efficiency suggests that the star-forming activity in

the central disk is increasing. In this sense the galaxy may be identified as being a pre-starburst galaxy just after the accretion of gas. Finally, we mention that the relationship between the star-burst and/or star forming activity and the ring formation/fission mechanisms is open to further investigation.

We thank Prof. M. Fujimoto of Nagoya University and Dr. M. Noguchi of the National Observatory for their critical reading of the manuscript and for the discussion. This work was financially supported in part by the Ministry of Education, Science, and Culture under Grant No. 61460009 (Y. Sofue).

References

Arp, H. 1966, in *Atlas of Peculiar Galaxies* (California Institute of Technology, California), p. 48.
Ball, R., Sargent, A. I., Scoville, N. Z., Lo, K. Y., and Scott, S. L. 1985, *Astrophys. J. Letters*, **298**, L21.
Combes, F. 1978, *Astron. Astrophys.*, **65**, 47.
Combes, F. 1988, in *Molecular Clouds in the Milky Way and External Galaxies*, ed. R. L. Dickman, R. L. Snell and J. S. Young (Springer-Verlag, Berlin), p. 443.
de Bruyn, A. G. 1977, *Astron. Astrophys.*, **58**, 221.
de Vaucouleurs, G., and de Vaucouleurs, A. 1963, *Astrophys. J.*, **137**, 363.
de Vaucouleurs, G., de Vaucouleurs, A., and Corwin, H. G., Jr. 1976, in *Second Reference Catalogue of Bright Galaxies* (Univ. Texas Monography in Astron.), p. 174.
Ekers, R. D., and Sancisi, R. 1977, *Astron. Astrophys.*, **54**, 973.
Fujimoto, M., and Sørensen, S. A. 1977, *Astron. Astrophys.*, **60**, 251.
Fukunaga, M. 1983, *Publ. Astron. Soc. Japan*, **35**, 173.
Handa, T., Nakai, N., Sofue, Y., Hayashi, M., and Fujimoto, M., 1990, *Publ. Astron. Soc. Japan*, **42**, No. 2, in press.
Hummel, E., Lesch, H., Wielebinski, R., Schlickeiser, R. 1988, *Astron. Astrophys.*, **197**, L29.
Huntley, J. M., Sanders, R. H., and Roberts, W. W., Jr. 1978, *Astrophys. J.*, **221**, 521.
Ishiguro, M., Kawabe, R., Morita, K.-I., Okumura, S. K., Chikada, Y., Kasuga, T., Kanzawa, T., Iwashita, H., Handa, K., Takahashi, T., Kobayashi, H., Murata, Y., Ishizuki, S., and Nakai, N. 1989, *Astrophys. J.*, **344**, 763.
Klein, U., Wielebinski, R., and Beck, R. 1984, *Astron. Astrophys.*, **133**, 19.
Kutner, M. L., and Ulich, B. L. 1981, *Astrophys. J.*, **250**, 341.
Lo, K. Y., Berg, G. L., Claussen, M. J., Heiligman, G. M., Leighton, R. B., Masson, C. R., Moffet, A. T., Phillips, T. G., Sargent, A. I., Scott, S. L., Wannier, P. G., and Woody, D. P. 1984, *Astrophys. J. Letters*, **282**, L59.
Lonsdale, C. J., Helou, G., Good, J. C., and Rice, W. L. 1985, in *Catalogued Galaxies and Quasars Observed in the IRAS Survey* (U.S. Government Printing Office, Washington, D.C.).
Nakai, N., Hayashi, M., Handa, T., Sofue, Y., and Hasegawa, T. 1987, *Publ. Astron. Soc. Japan*, **39**, 685.
Noguchi, M. 1987, *Monthly Notices Roy. Astron. Soc.*, **228**, 635.
Noguchi, M. 1988, *Astron. Astrophys.*, **203**, 259.
Oort, J. H. 1985, in *The Milky Way Galaxy, IAU Symp. No. 106*, ed. H. van Woerden and W. B. Burton (D. Reidel Publishing Company, Dordrecht), p. 349.
Parker, E. N. 1971, *Astrophys. J.*, **163**, 255.
Rubin, V. C., Ford, W. K., Jr., and Thonnard, N. 1980, *Astrophys. J.*, **238**, 471.
Sandage, A. 1961, in *The Hubble Atlas of Galaxies* (Carnegie Institution of Washington, Washington, D. C.), p. 25.
Sandage, A., and Tammann, G. A. 1974, *Astrophys. J.*, **194**, 559.
Sanders, D. B., Scoville, N. Z., Young, J. S., Soifer, B. T., Schloerb, F. P., Rice, W. L., and Danielson, G. E. 1986, *Astrophys. J. Letters*, **305**, L45.
Schlosman, I., Frank, J., and Begelman, M. C. 1989, *Nature*, **338**, 45.

Sofue, Y. 1988, in *Galactic and Extragalactic Star Formation*, ed. R. Pudritz and M. Fich (Kluwer Academic Publishers, Dordrecht), p. 409.
Sofue, Y., Doi, M., Ishizuki, S., Nakai, N., and Handa, T. 1988, *Publ. Astron. Soc. Japan*, **40**, 511.
Sofue, Y., Nakai, N., and Handa, T. 1987, *Publ. Astron. Soc. Japan*, **39**, 47.
Sørensen, S.-A., Matsuda, T., and Fujimoto, M. 1976, *Astrophys. Space Sci.*, **43**, 491.
Sukumar, S., and Velusamy, T. 1985, *Monthly Notices Roy. Astron. Soc.*, **212**, 367.
Tatematsu, Y., and Fujimoto, M. 1989, submitted to *Publ. Astron. Soc. Japan*.
Weliachew, L., Casoli, F., and Combes, F. 1988, *Astron. Astrophys.*, **199**, 29.
Weliachew, L., Sancisi, R., and Guélin, M. 1978, *Astron. Astrophys.*, **65**, 37.
Werner, W. 1985, *Astron. Astrophys.*, **144**, 502.
Young, J. S. 1988, in *Molecular Clouds in the Milky Way and External Galaxies*, ed. R. L. Dickman, R. L. Snell, and J. S. Joung (Springer-Verlag, Berlin), p. 326.
Young, J. S., Schloerb, F. P., Kenney, J. D., and Lord, S. D. 1986, *Astrophys. J.*, **304**, 443.
Young, J. S., and Scoville, N. 1982, *Astrophys. J.*, **258**, 467.